Design and aeroelastic analysis of truss-based modular wing structures

Silva, Higor Luis ; Machado Guimarães, Thiago Augusto ; Castro, Saullo G.P.

DOI
10.2514/6.2023-1677

Publication date
2023

Document Version
Final published version

Published in
AIAA SciTech Forum 2023

AIAA SciTech Forum
23-27 January 2023, National Harbor, MD & Online
AIAA SCITECH 2023 Forum

10.2514/6.2023-1677

Design and aeroelastic analysis of truss-based modular wing structures

Higor Luis Silva *
Federal University of Uberlândia, Uberlândia, MG, 38408-100, Brazil

Thiago Augusto Machado Guimarães †
University of Michigan, Ann Arbor, Michigan, 48109-2140

Saullo Giovani Pereira Castro ‡
Delft University of Technology, Kluyverweg 1, 2629HS Delft, The Netherlands

Modular structures come with the promise of efficient manufacturing and reduced maintenance costs. The amount of modularization is usually limited by weight efficiency, meaning that the minimum weight always lies on the most customized design, where all the structural elements are allowed to be different across the structural domain. This work studies a new design approach and structural and aeroelastic optimization of wings using truss-based modular structures. Furthermore, the work proposes a new approach to structural topology, eliminating traditional elements, such as spars and ribs, and replacing them with modular truss-based structures, which are connected by spherical joints at their ends. The topological mesh of the structures are created from the Delaunay triangulation and tessellation. The structural model is based on two types of finite elements: beam and quadrilateral elements. The beam elements are defined from consistent Timoshenko elements and the quadrilaterals are based on Mindlin-Reissner kinematics using bi-linear interpolation and reduced integration to prevent shear locking. The Doublet-Lattice Method is used to predict the unsteady subsonic aerodynamics, and the P-K method is used to compute the aeroelastic system solution. For the examples and case studies, a reference wing geometry from the FLEXOP project is used as a baseline. Two optimizations are proposed, where in all the objective functions are to minimize the structural weight of the wing and to maximize the flutter speed. The first optimization has as design variables the number of control points, or nodes, in each airfoil and the number of sections along the span. In the second optimization, the external diameters and thicknesses of each of the modular structures are individually optimized, even eliminating unnecessary ones. The results show that it is possible to obtain relatively light wings that meet the structural and aeroelastic requirements; however, the definition of the optimization parameters directly influence the mesh generation and computational cost of the optimization. Above all, modular structures have proved to be a good strategy in the design of structures for new wing concepts.

I. Introduction

In the last years, the aerospace industry has faced many challenges in the development of new projects and technological innovations [1]. With a global debate increasingly focused on environmental impacts and other climate changes, aviation as a whole could not be absent from the discussions, since it is one of the biggest contributors to the emission of greenhouse gases [2]. In this context, engineers and researchers have been dedicating efforts to develop increasingly efficient aircraft, i.e., aircraft that are increasingly lighter and that consume less fossil fuels [3–6]; however, to achieve very aggressive goals [7, 8], it is necessary to move forward and create new disruptive technologies [9–11].

Regarding fossil fuel consumption, in recent years many conceptual projects and experimental models have been presented to the market [12–18]. Hybrid-electric and fully-electric aircraft designs seek to combine innovative propulsion systems, including electric motors and batteries, in order to reduce energy consumption during a certain mission, which can make somehow some operations more profitable, such as the thin-haul operations [19]. However, most operations

*PhD Candidate, Department of Mechanical Engineering, Av. João Naves de Ávila 2121, AIAA Member. (higor@ufu.br)
†Visiting Professor, Department of Aerospace Engineering, 1320 Beal Avenue, Ann Arbor, MI, AIAA Member. (tmachado@umich.edu)
‡Assistant Professor in the group of Aerospace Structures and Computational Mechanics. (S.G.P.Castro@tudelft.nl)

are not yet benefited, since long-range missions require a lot of stored energy, which would imply tons of batteries [20]. Thus, the technological advancement of specific energy of batteries is still crucial [21]. In this context, other alternatives have been recently presented, such as the new Airbus hydrogen-powered airplanes [22]. These new concepts rely on hydrogen as a primary source, granting zero chemical emissions in all phases of flight [23], which enables advances towards decarbonization of the entire aviation industry, likely being a solution for aerospace and many other industries to meet their climate-neutral targets.

On the other hand, when it comes to more efficient aircraft, the idea of better aerodynamic efficiencies and lighter structures easily comes to mind. For better aerodynamic efficiency of next-generation aircraft concepts, many studies propose wings with higher aspect ratios and different design shapes, examples being the D8.x jet transport configuration [24] or the Truss-Braced Wing concept [25]. Moreover, Martins et al. [26] evaluate the impact of new structural material technologies on the aerostructural tradeoffs in the design of conventional and high aspect ratio wing design. Zhang et al. [27] design and compare sandwich multi-spar structures and innovative mixed structures basing on the structural characteristics of high aspect ratio wings. Furthermore, Afonso et al. [28] present a review on the state-of-the-art on nonlinear aeroealasticity of high aspect-ratio wings. At the same time, when designing aircraft wings with larger spans and with lighter structures, these wings tend to become less stiff and consequently more prone to aeroelastic instabilities such as flutter, which can render much of the operation envelope unfeasible. In this sense, aeroelastic constraints become important issues to take care of and account for during the design process, mainly in early design stages [29], preventing costly design changes in later design phases or worse during flight testing.

Some works have been studying new models of structure for the wing, presenting novel manufacturing techniques and enabling unconventional internal wing layouts. Saleem et al. [30] apply nonparametric topology optimization and manufacturing simulation on a commercial aircraft vertical stabilizer component. Sleesongsom et al. [31] propose a novel design approach for synthesizing the internal structural layout of a morphing wing. Nevertheless, when the topic is manufacturing, assembling, and optimization with design constraints, it is important to ensure that the structures can be easily handled and used on large scale. Thus, a good strategy is to divide the structure into a set of similar parts so that the process becomes less costly and easier to be reused, which in turn represents the concept of modularity. Therefore, modular structures have also been studied in aerospace applications because they present benefits analogous to truss topology. Following that, Montemurro et al. [32] present a two-level procedure for the global optimum design of composite modular structures, applying to the design of an aircraft wing. Moses et al. [33] suggest a numerical method for the topological design of modular structures under general and arbitrary loading.

Along those lines, this paper proposes a study of modularity and topology optimization of a wingbox structure, accounting for aeroelastic constraints. The modularity is addressed by using truss-based modular structures, looking for a tradeoff between topological mesh vs. weight. The wingbox model used as a baseline is from the FLEXOP project [34], which has an aspect ratio of 20 and a thin wingbox profile that poses even more challenges to the structural design. Two optimizations are proposed, where in all the objective functions are to minimize the structural weight of the wing and to maximize the flutter speed. The aeroelastic constraints are computed employing the P-K method coupled to the Doublet-Lattice Method (DLM), which is used to predict the unsteady subsonic aerodynamics. The optimizations are performed using genetic algorithms, where the design variables are the types of each modular structure and the arrangements. The first optimization has as design variables the number of control points, or nodes, in each cross-section, the number of cross-sections along the wingspan, and the diameter of all elements of modular structures. In the second optimization, the external diameters and thicknesses of each of the modular structures are individually optimized, even eliminating unnecessary ones. The optimizations are also performed using the well-known algorithm NSGA-II.

II. Formulation

A. Structural model

The structural model is based on two finite element types to correctly represent the different wing structural designs: quadrilateral and beam elements. The quadrilateral elements provide the necessary field representation to calculate the stresses at the skin region and are based on Mindlin-Reissner kinematics using bi-linear interpolation and reduced integration to prevent shear locking. The bi-linear interpolation is calculated based on the nodal positions of the element in local coordinates, where each i^{th} nodal position is given by x_i and y_i, such that:

$$N(x,y) = (x_1 + \frac{1}{2}(\eta+1)(-x_1+x_4+\frac{1}{2}(x_1-x_2)(\xi+1)+\frac{1}{2}(x_3-x_4)(\xi+1)) - \frac{1}{2}(x_1-x_2)(\xi+1))\boldsymbol{i} + (y_1 + \frac{1}{2}(\eta+1)(-y_1+y_4+\frac{1}{2}(\xi+1)(y_1-y_2)+\frac{1}{2}(\xi+1)(y_3-y_4)) - \frac{1}{2}(\xi+1)(y_1-y_2))\boldsymbol{j} \quad (1)$$

such that the values of the interpolation function at the nodes N_1, N_2, N_3, N_4 can be calculated by respectively replacing ξ, η by: $(-1,-1)$, $(+1,-1)$, $(+1,+1)$ and $(-1,+1)$. The hour-glass control is implemented according to Brockman [35], where the second derivatives of the bi-linear interpolation functions are used to define generalized hourglass strain components that apply to each translational degree-of-freedom: ε_h^u, ε_h^v, and ε_h^w; and generalized hourglass strains that apply to two rotational degrees-of-freedom: $\varepsilon_h^{r_x}$, $\varepsilon_h^{r_y}$; noting that no hourglass strain or stiffness is added to the drilling degree-of-freedom r_z. A generalized hourglass stiffness is defined for each generalized hourglass strain. Because Brockman's work is based on metallic structures, the originally proposed generalized hourglass stiffnesses need to be modified to account for laminated composite plates as follows:

$$E_h^u = \frac{0.1E_{1eq}h}{1.0+1.0/A_e} \quad (2)$$

$$E_h^v = \frac{0.1E_{2eq}h}{1.0+1.0/A_e}$$

$$E_h^{r_x} = \frac{0.1E_{2eq}h^3}{1.0+1.0/A_e}$$

$$E_h^{r_y} = \frac{0.1E_{1eq}h^3}{1.0+1.0/A_e}$$

$$E_h^w = \frac{1}{2}(E_h^{r_x} + E_h^{r_y})$$

where A_e is the area of the quadrilateral element; h is the total thickness of the element; $E_{1eq} = 1/(ha_{11})$ and $E_{2eq} = 1/(ha_{22})$ with a_{11} and a_{22} components of the flexibility matrix of the laminated composite plate. The variation of the hourglass strain energy δU_h is therefore given by the integral:

$$\delta U_h = \bar{\boldsymbol{u}}_{\boldsymbol{e}}{}^{\top} \iint_{x,y} \left(\boldsymbol{N}_h^{u\top} E_h^u \boldsymbol{N}_h^u + \boldsymbol{N}_h^{v\top} E_h^v \boldsymbol{N}_h^v + \boldsymbol{N}_h^{w\top} E_h^w \boldsymbol{N}_h^w + \boldsymbol{N}_h^{r_x\top} E_h^{r_x} \boldsymbol{N}_h^{r_x} + \boldsymbol{N}_h^{r_y\top} E_h^{r_y} \boldsymbol{N}_h^{r_y} \right) dxdy \;\; \delta\bar{\boldsymbol{u}}_{\boldsymbol{e}} \quad (3)$$

which is then added to the strain energy ultimately contributing to the constitutive stiffness matrix of the system. The drilling degree-of-freedom is calculated simply by penalizing the in-plane rotational shear, as for instance discussed in Adam et al. [36]. Here, the drilling stiffness $E_{drilling}$ is calculated based on the laminated composite plate stiffness component A_{66}, such that:

$$E_{drilling} = \frac{A_{66}}{h} \quad (4)$$

The truss-based regions that replace the spars, ribs, and stiffeners of a conventional wing design are represented using a consistent Timoshenko beam element, with the formulation proposed by Luo [37]. This formulation has been implemented without modifications, and the reader is referred to Luo's reference for further details. Furthermore, the formulation presented is already implemented in Python and available as a library named `pyfe3d`, which has been developed by Castro [38]. Therefore, the mass and stiffness matrix of the wing structure under analysis are obtained by using that library package.

B. Aerodynamic model

For the aerostructural coupling, the Doublet Lattice Method (DLM) is used to predict the unsteady subsonic aerodynamics. According to the mission of the reference This method was first developed by Albano and Rodden [39] to calculate the lift distributions in the subsonic flow region. Subsequent work was done, for example, by Geising et al. [40], to refine the calculation ability on nonplanar or noncoplanar surfaces and to improve the modeling of wing-fuselage interference [41].

The behavior of small perturbations of the velocity potential ϕ in an inviscid, rotational, and compressible flow, linearised around a uniform, parallel flow with velocity U_∞ along x is described by the governing Partial Differential Equation (PDE):

$$(1 - M_\infty^2)\tilde{\phi}_{xx} + \tilde{\phi}_{yy} + \tilde{\phi}_{zz} - \frac{2U_\infty}{a_\infty^2}\tilde{\phi}_{xt} - \frac{1}{a_\infty^2}\tilde{\phi}_{tt} = 0 \tag{5}$$

with a_∞ the speed of sound in the far-field flow, and $M_\infty \equiv U_\infty/a_\infty$ the corresponding Mach number. The boundary conditions needed to solve the PDE follow from the unperturbed flow condition at infinity and tangential flow over the lifting surface S,

$$\tilde{\phi}|_{\text{far-field}} = 0 \qquad \text{and} \qquad \frac{\partial S}{\partial t} + \nabla\tilde{\phi} \cdot \nabla S = 0 \tag{6}$$

where the latter condition holds only on S. The tilde denotes time-dependent perturbation to the steady far-field flow $\bar{\phi} = U_\infty x$.

The pressure differential induced by an infinitesimal element of the acceleration potential doublets sheet is related to its strength A_Ψ as

$$\Delta\bar{p} = 4\pi\rho_\infty A_\Psi \mathrm{d}\xi\mathrm{d}\sigma \tag{7}$$

with ξ and σ the tangential coordinates. Then, integrating Eq. (7) over a sheet S of pressure doublets and dividing by U_∞, the integral equation in non-dimensional form is obtained:

$$\frac{\bar{w}_N}{U_\infty} = \frac{-1}{4\pi\rho_\infty U_\infty^2}\iint_S \Delta\bar{p}(\xi,\eta,\zeta)K(x-\xi, y-\eta, z-\zeta)\mathrm{d}\xi\mathrm{d}\sigma \tag{8}$$

where K is the so-called Kernel Function, expressed by:

$$K(x_0, y_0, z_0) \equiv \exp\left[\frac{i\omega x_0}{U_\infty}\right]\frac{\partial}{\partial N_r}\frac{\partial}{\partial N_s}\int_{-\infty}^{x_0}\frac{1}{R'}\exp\left[i\omega\frac{\lambda - M_\infty R'}{U_\infty\beta_\infty^2}\right]\mathrm{d}\lambda \tag{9}$$

with the relative coordinate system (x_0, y_0, z_0) defined as $x_0 \equiv x - \xi$, $y_0 \equiv y - \eta$, and $z_0 \equiv z - \zeta$. The integral formula (8) relates the unknown pressure differential $\Delta\bar{p}$ generated by a thin lifting surface, modeled as a sheet of acceleration potential doublets, to the velocity normal to the surface $\bar{w}_N$ (normalwash) in a receiving point.

Regarding the geometry idealization, Albano and Rodden [39] originally proposed to divide the geometry into n_{tot} of trapezoidal elements (Fig. 1), referred to as boxes or panel, aligned chord-wise with the far-field flow and over which the pressure is assumed constant.

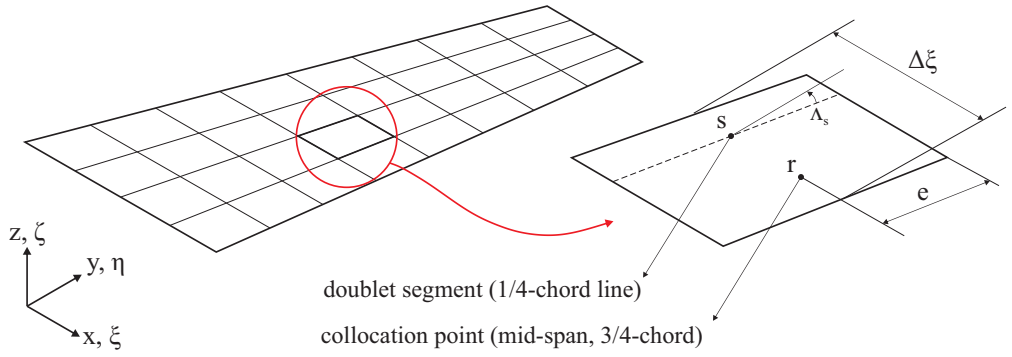

Fig. 1 Discretization of the lifting surface geometry and overview of the panel.

In view of this discretization, the integral equation (8) for the induced normalwash at a receiving panel r becomes a sum of the contributions from each emitting panel s, or

$$\frac{\bar{w}_{N,r}}{U_\infty} = \sum_s \frac{-\Delta\bar{p}_s \Delta x_s}{4\pi\rho_\infty U_\infty^2} \iint_s K(x-\xi, y-\eta, z-\zeta)\mathrm{d}\xi\mathrm{d}\sigma \tag{10}$$

$$= \sum_s -\Delta\bar{c}_{p,s} \frac{\Delta x_s}{8\pi} \iint_s K(x-\xi, y-\eta, z-\zeta)\mathrm{d}\xi\mathrm{d}\sigma \tag{11}$$

with Δx_s the chord of the emitting panel and $\delta\bar{c}_{p,s}$ the non-dimensional pressure coefficient, $\Delta\bar{c}_{p,s} = \Delta\bar{p}_s/0.5\rho_\infty U_\infty^2$. In addition, the influence of the doublet sheet over each element s is lumped onto a span-wise segment along the 1/4-chord line. The flow properties are evaluated at collocation or control points placed at the midspan of the 3/4-chord line.

Thus, the previous expression may be cast into the linear system

$$\{\bar{w}_N\} = [D]\,\{\Delta\bar{c}_p\} \qquad \text{or} \qquad \bar{w}_{N,r} = \sum_{s=1}^{n_{\text{tot}}} D_{rs}\Delta\bar{c}_{p,s} \tag{12}$$

where the $n_{\text{tot}} \times n_{\text{tot}}$ matrix $[D]$ relating the lifting pressure at a panel s to the normalwash at some other panel r, is the so-called matrix of total downwash factors.

The basic idea in the Doublet-Lattice method is to adjust a polynomial, usually of the second or fourth degree, to the numerator of the Kernel Function (9), allowing an analytical integration. The K function, however, has an exact steady contribution that can be integrated analytically without any adjustment. So one way to increase the accuracy of the method is to separate the steady and unsteady contributions in the Kernel numerator. With these strategies, it can be shown that each element of matrix $[D]$ is given by

$$D_{rs} = D_{rs}^{(0)} + D_{rs}^{(1)} + D_{rs}^{(2)} \tag{13}$$

where the superscripts $^{(0)}$, $^{(1)}$ and $^{(2)}$ denote, respectively, the steady, planar unsteady, and non-planar unsteady contributions.

C. Aeroelastic Constraints

In order to solve the aeroelastic system equations for the flutter problem, it is interesting to transform the equation of the dynamics of movement into a modal system. Since flutter approximates the natural frequencies of the structure, it is convenient to evaluate the evolution of instability from mode to mode. Thus, the aerodynamic load calculated at the points defined by an aerodynamic mesh is given by:

$$\{L_a\} = q_\infty \{T_{as}\}^T\,[S]\,\{w_N\}\,[AIC]\,\{T_{as}\}\{h_{\text{modal}}\} \tag{14}$$

where $[AIC] = [Drs]^{-1}$ is the matrix of aerodynamics influence coefficients. Similarly, the generalized aerodynamic load, Q_j, that is, the reduced load on the j-th modal base, is given by:

$$\left[Q_j\right] = \{\Phi_j\}^T \{T_{as}\}^T\,[S]\,\{w_N\}\,[AIC]\,\{T_{as}\}\{\Phi_j\} \tag{15}$$

where Φ_j is the j-th mode of vibration, obtained through the eigenvalue and eigenvector solution from the FEM. Eq. (15) represents the calculation of the so-called generalized aerodynamic matrix (GAM), which is a complex matrix based on the Mach number and the reduced frequency, derived from the matrix (AIC), and reduced on the modal basis. The aeroelastic analysis assumes that complex loading can be separated in real and imaginary terms, denoting, respectively, the aerodynamic influence on the damping and rigidity of the system. Thus, the generalized motion equation can be written as follow:

$$\left[M_q\right]\{\ddot{q}\} + \left[K_q\right]\{q\} = \frac{\rho V}{2}\,[Q_I]\,\{\dot{q}\} + \frac{\rho V^2}{2}\,[Q_R]\,\{q\} \tag{16}$$

Equation (16) is the aeroelastic equation of the system described in modal coordinates. It can be represented in the classic aeroelastic form described by Wright and Cooper [42] as

$$\mathbf{A}\ddot{q} + \rho V\mathbf{B}\dot{q} + \left(\rho V^2\mathbf{C} + \mathbf{E}\right) q = 0 \tag{17}$$

where **A** is the modal mass matrix, **B** the aerodynamic damping matrix due to the flow, **C** the aerodynamic stiffness matrix, and **E** the structural stiffness matrix, with the aerodynamic terms dependent on the reduced frequency.

Since the aerodynamic damping and stiffness matrices are dependent and vary with reduced frequency, the aeroelastic system solution is obtained through well-established iterative methods in the literature, such as the PK method [43], which is used here. So, having the aeroelastic equation (16) as a non-linear eigenvalue problem, assuming that $p \equiv \mathrm{d}/\mathrm{d}t$, then $\ddot{q} = p^2 q$:

$$\left(p^2 \left[M_q\right] + \left[K_q\right] - \frac{\rho V^2}{2} \left[Q(k)\right]\right) \{q\} = 0 \tag{18}$$

From the eigenvalue problem, described by Eq. (7), the complex root $p = \omega\,(\gamma \pm i)$ is determined. The dynamic characteristics of the aeroelastic system, such as frequency and damping, are computed as follows:

$$\omega = \mathrm{Im}\,(p) \tag{19}$$

$$g = 2\gamma = 2\mathrm{Re}\,(p)\,/\mathrm{Im}\,(p) \tag{20}$$

Based on the values of ω and g, it is possible to verify the stability of the dynamic system (stable for negative values of g). The critical flutter and divergence speeds are obtained in the vicinity of the unstable responses ($g = 0$). While flutter is characterized by the coalescence between two vibration modes (fluid-structure problem), the divergence is determined when the natural frequency tends to zero.

III. Wing Design Approach and Optimizations

The work of Opgenoord and Willcox [44] investigated what the authors called lattice structures in the design of wing structures. The authors focused on additive-manufactured elements, therefore not constrained by modularity requirements.

The wing designed in this work is based on the premise that modular structures will be used in its formation, that is, instead of traditional and conventional structures such as spars and ribs, truss-based modular structures will be used here. In other words, all internal wing-box components, except for the upper and lower skins, are replaced by truss-based structural elements. Thus, to do so, the trusses forming the lattice structure are defined from a catalog of possible cross-sections, and the number of possibilities in this catalog defines the level of modularity of the design.

In this sense, to make the necessary connections between the modular structures, this work discretizes the wing as follows. First, as there are no ribs that form the airfoil, control points are used at each cross-section. These control points are defined by means of a spline in order to guarantee the selected aerodynamic profile. In the implementation, for example, the definition of the points starts from the choice of the airfoil profile and the number of points to form the spline. Furthermore, it is possible to determine if the trailing edge will be formed by only one point and if the spacing between the points will follow a half-cosine-based spacing. As an example, Fig. 2 depicts the spline and the corresponding control points for a profile NACA 2412 with 8 and 20 points, respectively. It is worth mentioning that those control points are going to be the nodes of the FEM model and the connection nodes of all elements.

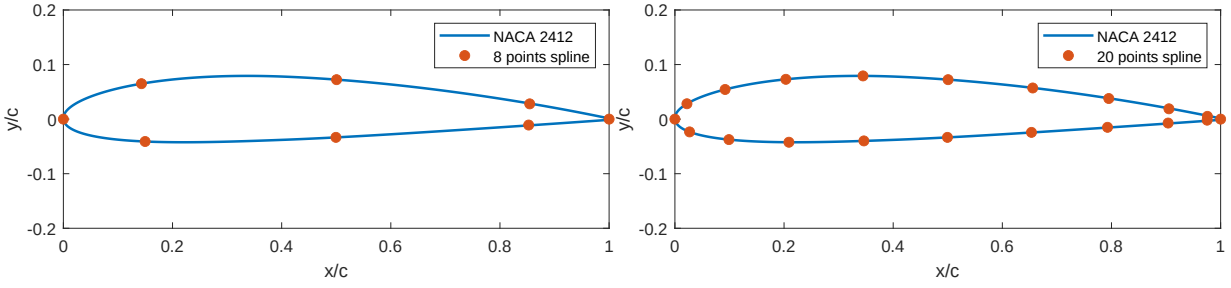

(a) 8 points spline.

(b) 20 points spline.

Fig. 2 Cross-section discretizations for NACA 2412.

Furthermore, instead of the conventional spars, the proposal here is to use truss-based modular structures. However, defining the spatial arrangement of such structures is the big deal. Therefore, to create the structural mesh, this works makes use of the Delaunay Tessellation, i.e., the Delaunay Triangulation and Tetrahedrization to connect the cross-section nodes and so create the maximum truss elements without physically crossing them.

Delaunay's algorithm is a finite element meshing process that has the ability to consistently subdivide the geometric domain into simplexes. Simplexes are extensions of triangles in other dimensions, i.e., line segments in one dimension, tetrahedrons in three-dimensional space, etc. Therefore, having the Delaunay Triangulation and Tetrahedrization stated, the wing structural mesh is designed from the control points defined in each cross-section. Therefore, as an example, the structural meshes for a wing of 10 cross-sections and considering 8 (as in Fig. 2a) and 20 (as in Fig. 2b) control points in each cross-section are shown in Fig. 3a and 3b, respectively.

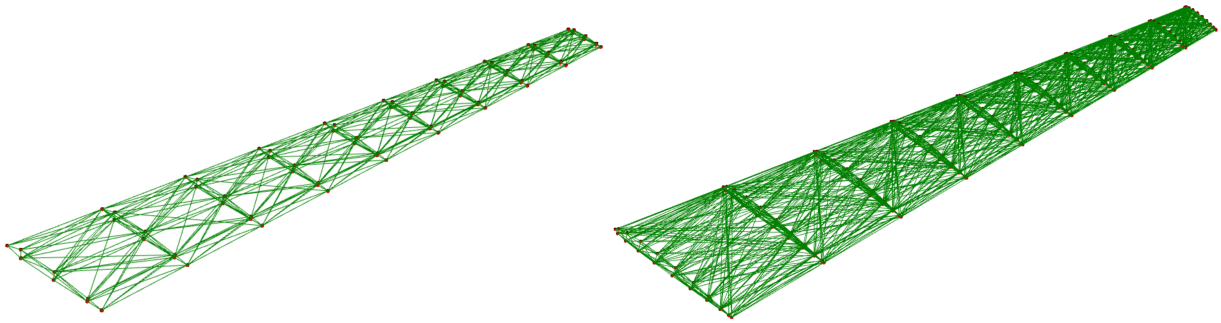

(a) 8 points spline.

(b) 20 points spline.

Fig. 3 Truss-based structural meshes for 8 and 20 control points in each cross-section, respectively.

Regarding the joints, this work did not have the objective of designing them; however, in the aeroelastic system, it is important to consider the weight of the joints at the nodes, since it affects the total weight of the structure and even the dynamic behavior of the structure. Therefore, for this work, it was assumed a reasonable mass of 150 g for each joint in the structure. It is worth mentioning that in the sequence of this work it is intended to consider the joint design together with the wing design, as well as to take geometric connections as a constraint in the optimization of the truss elements, i.e., the angles between the elements in the joints will be considered as a design constraint.

The reference wing geometry comes from the flying demonstrator of the FLEXOP project (Flutter Free FLight Envelope eXpansion for ecOnomical Performance improvement) [34, 45]. The demonstrator is shown in Fig. 4 and the structural layout of the wing and its main geometric parameters are given in Fig. 5 and Table 1. The high aspect ratio of 20 and thin airfoil profile makes the lightweight structural design especially challenging, given the low second area moment of inertial of the wingbox and the large bending loads at the wing root.

Fig. 4 FLEXOP flight demonstrator, from [45].

At this point, it is worth summarizing the wing design approach of this work. First, it uses the dimensions and geometry of the FLEXOP wing planform. Second, the number of cross-sections along the wingspan is chosen. Next, the number of control points (nodes) in each of the cross-sections is defined. Finally, a spatial mesh/arrangement of modular structures is created using the Delaunay tessellation method.

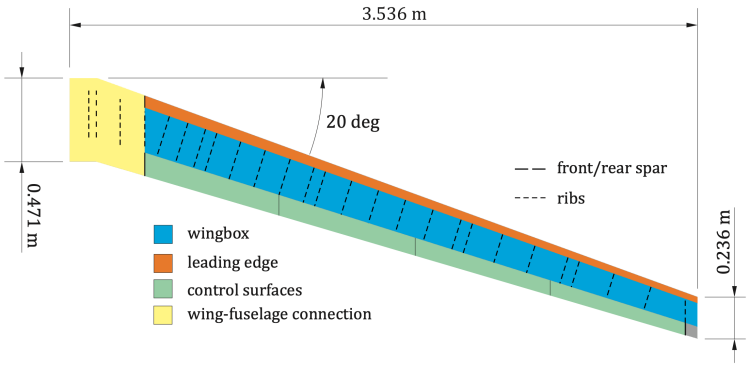

Fig. 5 Wing structural layout, from [34].

Table 1 Geometric parameters for the FLEXOP reference wing, from [34].

Parameter	Value
Semi-span	3.536 m
Aspect ratio	20
Chord, root	0.471 m
Chord, tip	0.236 m
Thickness, root	10% chord
Thickness, tip	8% chord
Sweep, leading edge	20 deg

Thus, the structural model is then created, and, using the DLM, it is possible to obtain the unsteady aerodynamic loads, extract the mass and stiffness matrices and vibration modes from the modal analysis, and perform the aerostructural coupling, obtain the flutter solution and verify the aeroelastic stability condition.

The reader may have noticed that the definition of the number of cross-sections and the number of control points (nodes) in each cross-section directly affects the number of modular structures created by Delaunay's spatial tessellation. Furthermore, the wing design proposal in this work is to generate the lightest possible wing using modular structures, but accounting for structural and aeroelastic constrains. Therefore, it is necessary to think from an optimization point of view, that is, what is the best combination of design variables that generate such results and, finally, to study the trade-off of benefits through the Pareto curves obtained by the optimizations. The optimization method applied is presented in the next chapter.

A. Optimization #1

The design will seek for minimizing the structural weight of the wing (W_{wing}) and maximizing the flutter speed ($V_{flutter}$), taking into consideration structural and aeroelastic constraints.

Along those lines, for the first optimization case, the following parameters are stated as design variables: the number of control points (nodes) in each cross-section of the wing ($n_{\text{control points}}$), the number of cross-sections distributed along the wingspan ($n_{\text{cross-sections}}$), and the diameter of all elements of modular structures (D_{bar}), which are considered here as solid truss bars.

To get started, the search range of the design variables, i.e., the intervals of values for optimization for $n_{\text{control points}}$, $n_{\text{cross-sections}}$, and D_{bar} go from 8 to 32, 6 to 14, and 3 to 10 mm, respectively. Thus, the multi-objective optimization problem #1 is summarized as follows:

$$\textit{Multi-objective optimization problem \#1} : \begin{cases} \min\left(W_{wing}\right) \quad \text{and} \quad \max\left(V_{flutter}\right) \\ \mathbf{x} : [n_{\text{control points}},\ n_{\text{cross-sections}},\ D_{\text{bar}}] \\ 8 \leq n_{\text{control points}} \leq 32 \\ 6 \leq n_{\text{cross-sections}} \leq 14 \\ 3 \leq D_{\text{bar}} \leq 10 \quad [\text{mm}] \end{cases}$$

Using the NSGA-II algorithm, the optimization was executed with a number of population of 100 and generations equal to 1000. The crossover index (η_c) and the mutation index (η_m) are defined as 3.0 and 3.0, respectively.

Furthermore, the aeroelastic constraint is accounting for the flutter speed and divergence speed. The p-k method is evaluated from 0 to 200 m/s with an increment in speed (ΔV) of 0.1 m/s. The skin applied to the structure has a thickness (t_{skin}) of 1 mm. Regarding the structural constraints, it is evaluated for the truss bars the Yield strength and Euler's critical load with a safety factor (FS) of 1.5. It is worth mentioning that the skin buckling is not evaluated in this work. Moreover, both the element types, i.e., truss bars and skin are assumed as made of Aluminum 7075 Heat Treated (T6), whose main properties include a modulus of elasticity (E) of 71.7 GPa, Poisson ratio of 0.33, and density of 2795.7 kg/m^3.

The optimization algorithm was run using Spyder, an IDE for Python, and on a computer with a processor 11th Gen Intel Core i7-1165G7 @ 2.80GHz, 16 GB of RAM, 512 GB of SSD, and the solution took around 156 hours to complete. Thus, the solution for the optimization problem #1 is given by the Pareto-optimal front depicted in blue circles in Fig. 6.

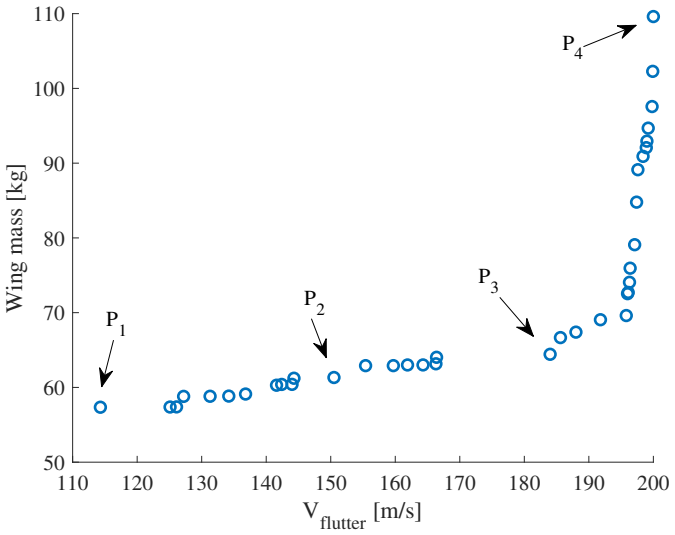

Fig. 6 Pareto front for Optimization #1.

As one can see, the result in Fig. 6 shows that to maximize the flutter speed, targeting a better aeroelastic behavior, there is an impact on the structural weight of the wing. Also, the feeling is mutual, i.e., it is possible to have a lighter wing, but the flutter speed is compromised. This trade-off is important in aircraft design, after all, the choice of design variables defines the structural behavior and affects the overall aircraft weight. Regarding the design variables, the NSGA-II found different combinations that delivered that result. The $n_{\text{control points}}$ varied from 8 to 26, $n_{\text{cross-sections}}$ from 6 to 14, and D_{bar} varied from 3 to 9 mm.

Also in Fig. 6, four points were selected: P_1, P_2, P_3, and P_4. These points represent four different options for the wing design. P_1 is the case where the wing has the lowest weight and worst flutter speed in that range. At the other end, P_4 is the case where the aircraft has the highest weight and best flutter speed in that range. The other points between P_1 and P_4 have different combinations of the design variables. The details of the wing design optimization for the four points selected are displayed in Table 2 and the corresponding structures are depicted in Fig. 7.

Table 2 Results of the design variables in optimization #1 for points P_1, P_2, P_3 and P_4 from Fig 6.

Parameter	P_1	P_2	P_3	P_4
$n_{\text{control points}}$	8	8	16	24
$n_{\text{cross-sections}}$	6	11	14	9
D_{bar} [mm]	3	5	4	7
$V_{flutter}$ [m/s]	114.3	150.6	184.2	199.9
Wing mass [kg]	57.23	61.18	64.21	109.74

Moreover, the flutter solutions for all four points are shown in Fig. 8 in terms of v-g-f diagrams. As one may notice, each structural mesh results in different modes, since there are different number of elements and also the diameter of the elements change over the optimization. Also, the mode of flutter onset changes among the four points; for example, for P_1, the v-f graphic shows a coupling of modes 1 and 2 (bending and torsion, respectively), while v-g graphic shows that mode 2 becomes unstable at 114.3 m/s. On the other hand, for P_2, the v-f graphic shows a coupling of modes 4 and 5, resulting in a flutter speed of 150.6 m/s.

At this point, it is possible to imagine and intuitive to say that considering all the modular structures in the

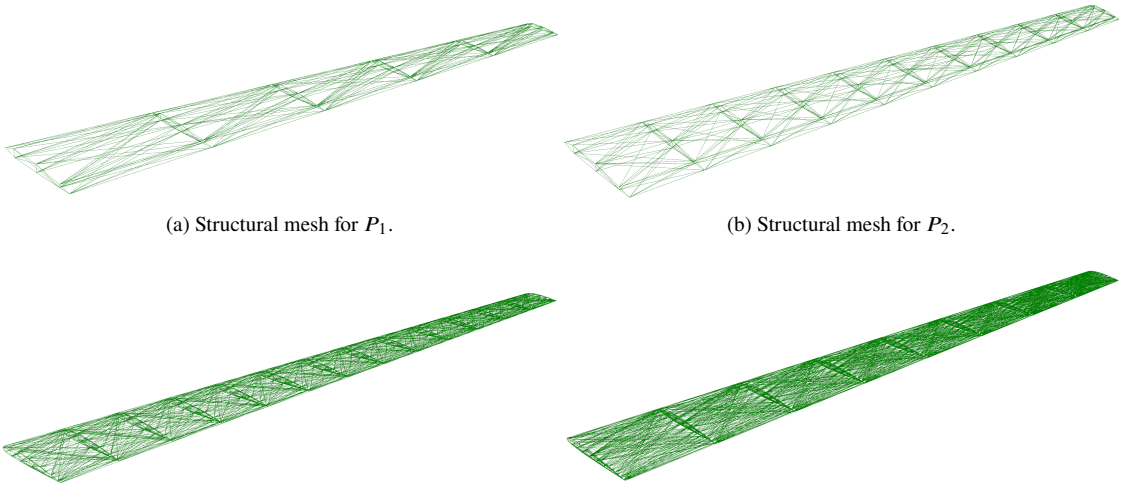

(a) Structural mesh for P_1.

(b) Structural mesh for P_2.

(c) Structural mesh for P_3.

(d) Structural mesh for P_4.

Fig. 7 Structural mesh of the truss-based wings obtained in P_1, P_2, P_3 and P_4.

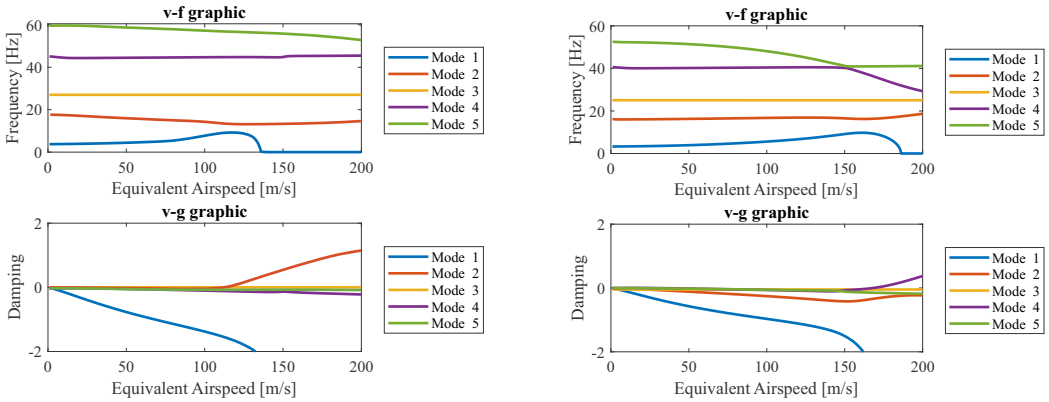

(a) V-g-f diagram for P_1.

(b) V-g-f diagram for P_2.

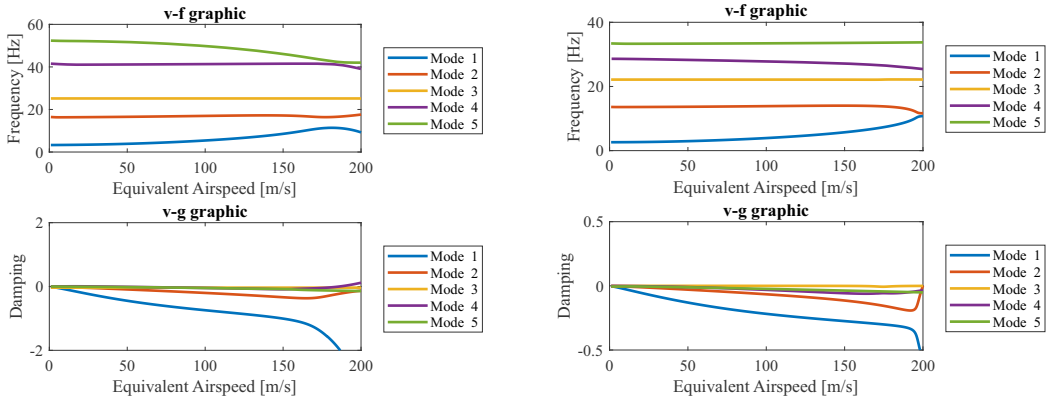

(c) V-g-f diagram for P_3.

(d) V-g-f diagram for P_4.

Fig. 8 Flutter solutions for points P_1, P_2, P_3 and P_4.

mesh/tessellation created by the Delaunay method does not represent the most efficient wing in terms of weight; after all, the more control points and/or number of cross-sections, more structures are inserted into the model, but many of these structures are unnecessary, that is, their removal would not affect the aeroelastic response, but would reduce the weight of the structure. Furthermore, the truss-based elements do not have to be solid bars, but tubular structures, which represents a considerable weight reduction. So, individually evaluating the inclusion or not of each element is a condition for a new optimization, which is presented in the next section.

B. Optimization #2

In Optimization #1, the wing design was performed considering an optimization in terms of $n_{\text{control points}}$, $n_{\text{cross-sections}}$, and D_{bar}. However, it is not very efficient to consider all the modular structures as solid bars. Therefore, at this point, the objective is to optimize all the modular elements individually; in other words, the optimization will try to eliminate some elements and will check how the resultant weight and aeroelastic behavior are.

At first sight, it is important to consider another constraint. The optimizer can not eliminate any element randomly. It is important to ensure at least the elements that form the airfoil shape and the wing planform; otherwise, the optimizer would try to eliminate any structural element that does not encounter any load path, and it could result in an inconsistent and unfeasible structural wing model. Therefore, the such constraint is required to establish the minimum wing profile is ensured.

The optimizer will design the wing eliminating or not the lattice elements. In addition, the outer diameter and tubular thickness of each individual element will be optimized. As one can imagine, to do so, it is necessary to know the number of lattice elements in the structure in order to optimize them, and, to know this number, it is necessary to previously define the number of control points (nodes) in each cross-section and the number of cross-sections along the wingspan. Only then it is possible to obtain the number of optimization variables. For example, $n_{\text{control points}} = 8$ and $n_{\text{cross-sections}} = 10$, the lattice created by the Delaunay approach results in 690 truss elements. If only the $n_{\text{cross-sections}}$ were increased to 11, the lattice results in 766 truss elements. Therefore, if the optimizer were also to optimize both parameters, i.e., $n_{\text{control points}}$ and $n_{\text{cross-sections}}$, it would result in an optimizer inside of another optimizer, which would result in an unreasonable computing cost.

Having that said, it is important to first define the values of $n_{\text{control points}}$ and $n_{\text{cross-sections}}$. Since both parameters can vary in a range of possibilities, the approach here is to select some pairs of those values in order to investigate how the optimization evolves with changing parameters. Thus, the multi-objective optimization problem #2 is summarized as follows:

$$\textit{Multi-objective optimization problem \#2} : \begin{cases} \text{Define: } n_{\text{control points}},\ n_{\text{cross-sections}} \\ \min\left(W_{wing}\right) \quad \text{and} \quad \max\left(V_{flutter}\right) \\ \mathbf{x} : [D_{i_{\text{ext,tube}}}, t_{i_{\text{tube}}}] \quad \text{for } i = 1, 2, \ldots, N_{\text{truss elements}} \\ D_{i_{\text{ext,tube}}} = 10, 15 \text{ or } 20 \quad [\text{mm}] \\ t_{i_{\text{tube}}} = 2, 4 \text{ or } 6 \quad [\text{mm}] \end{cases}$$

For this work, three pairs of values of $n_{\text{control points}}$ and $n_{\text{cross-sections}}$ were chosen. First, the optimization will run assuming a $n_{\text{control points}}$ equals to 8 and $n_{\text{cross-sections}}$ equals to 10. These values were chosen to ensure at least the minimum shape of the wing. Next, in the second optimization, the $n_{\text{control points}}$ is increased from 8 to 14, and $n_{\text{cross-sections}}$ is kept as 10. Then, in the third optimization, the $n_{\text{control points}}$ is kept as 14, and $n_{\text{cross-sections}}$ is increased from 10 to 20. All three pairs of configurations generate different numbers of elements and design variables, which are summarized in Tab. 3.

Table 3 Values for $n_{\text{control points}}$ and $n_{\text{cross-sections}}$ and the corresponding number of elements.

	$n_{\text{control points}} = 8$ $n_{\text{cross-sections}} = 10$	$n_{\text{control points}} = 14$ $n_{\text{cross-sections}} = 10$	$n_{\text{control points}} = 14$ $n_{\text{cross-sections}} = 20$
Number of truss elements	345	630	1309
Number of design variables	690	1260	2618

Similarly to what was done in Optimization #1, the aeroelastic constraint is accounting for the flutter speed and divergence speed. In contrast, the P-K method here is also evaluated from 0 to 200 m/s, but with an increment in speed (ΔV) of 1 m/s. The increment was increased from 0.1 to 1 m/s, when compared to Optimization #1, due to the computational cost to get the optimization done. The skin applied to the structure has a thickness (t_{skin}) of 1 mm. Regarding the structural constraints, it is evaluated for the truss bars the Yield strength and Euler's critical load with a safety factor (FS) of 1.5. It is worth mentioning that the skin buckling is not evaluated in this work. Moreover, both the element types, i.e., truss bars and skin are assumed as made of Aluminum 7075 Heat Treated (T6), whose main properties include a modulus of elasticity (E) of 71.7 GPa, Poisson ratio of 0.33, and density of 2795.7 kg/m^3.

The optimization algorithm was run using Spyder, an IDE for Python, and on a computer with a processor 11th Gen Intel Core i7-1165G7 @ 2.80GHz, 16 GB of RAM, 512 GB of SSD, and each solution took around 84 hours to complete. Thus, the solutions for the optimization problem #2 is given by three Pareto-optimal fronts depicted in Fig. 9.

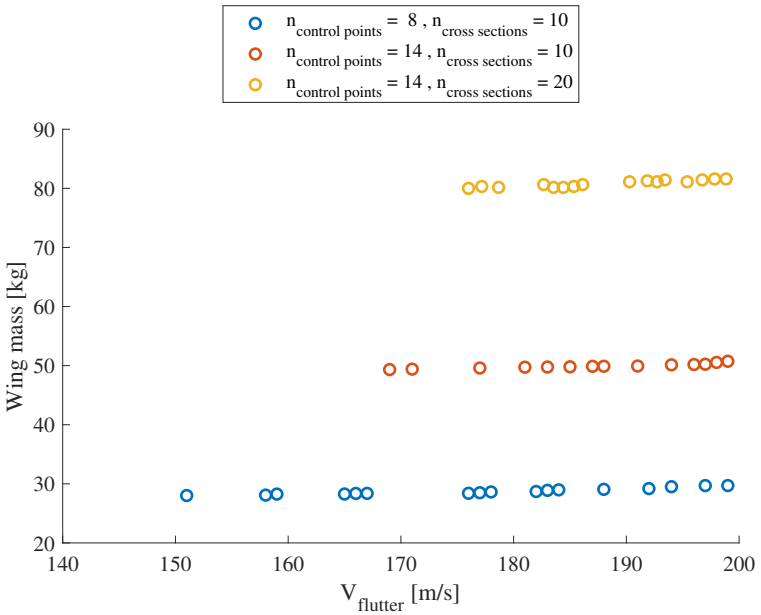

Fig. 9 Pareto fronts for Optimization #2.

From Fig. 9, the three Paretos show different wing designs for the problem previously defined. It is worth mentioning that there are few points in the Paretos. This happens because the flutter solution (p-k method) used in the optimization considered a speed increase of 1 m/s. So, the flutter speeds were always approximated by integer values, which made the Pareto ranking criterion eliminate the individuals that had the highest wing mass for each speed. Therefore, if a speed increment of 0.1 m/s were used, for example, there would probably be more points along each Pareto, but the computational cost would increase exponentially. Anyway, such solutions are sufficient for the purpose of this work, which is to verify the structural and aeroelastic design of the wing through optimization.

Furthermore, in Fig. 9 it is possible to see that the range of flutter velocities decreases as the discretization increases, i.e., the number of elements on the wing. This happens because the greater number of elements stiffens the wing and increases its weight, thus increasing the flutter speed. Speaking of weight, as the amount of elements increases, the weight increases considerably. It is worth remembering that the optimizer tried in its 1000 generations to eliminate as many unnecessary elements as possible, but even so, the increase in weight is quite considerable, since, for the same flutter speeds, a lighter wing is achieved (Pareto in blue). What influences in this case is how the optimizer defined the internal arrangement of each structure.

In this sense, selecting only the Pareto in blue from Fig. 9, since it brings the greatest cost-benefit in terms of structural weight and aeroelastic behavior, the vertically expanded Pareto is obtained in Fig. 10.

From Fig. 10, it is possible to verify only a small change in weight along the y-axis, while there is a considerable gain in flutter speed along the x-axis. Each point of that Pareto represents a different combination of design variables, which in this case it means a different combination of outer diameter and tubular thickness. Also, even if the number

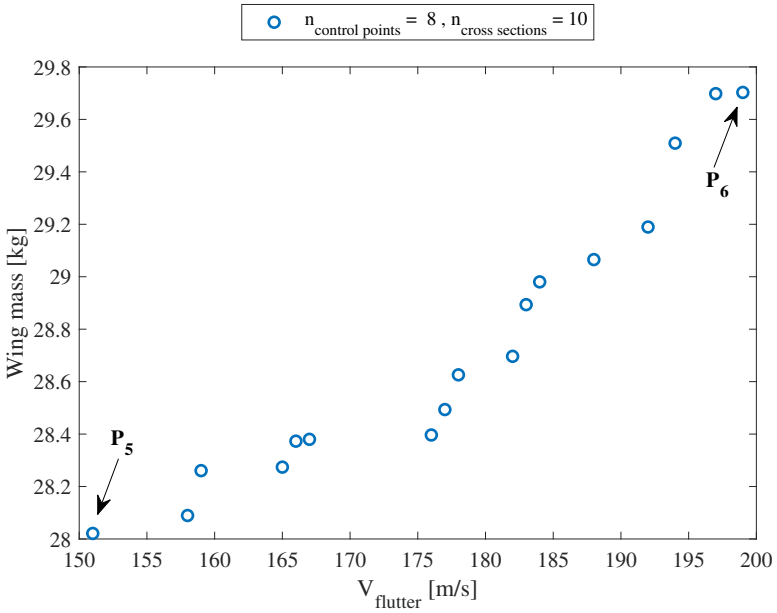

Fig. 10 Pareto front for $n_{\text{control points}} = 8$ and $n_{\text{cross-sections}} = 10$ from Fig. 9.

of nodes in the wing structure is the same for all Pareto points, since the number of nodes is defined by the value of $n_{\text{control points}} = 8$ and $n_{\text{cross-sections}} = 10$, each resulting wing at each point will have different numbers of elements, as the optimizer seeks to eliminate structural elements that it identifies as not necessary, that is, their absence does not violate any structural or aeroelastic condition.

Moreover, in Fig. 10, two points are chosen to exemplify in this analysis: P_5 and P_6. Comparing the cost-benefit in terms of structure mass and flutter velocity, one may notice that point P_6 offers a more interesting trade-off; in other words, it can be said that the most convenient design point, in this case, is the point P_6. After all, compared to the lower left point (P_5), the flutter speed has increased by almost 50 m/s ($\approx +33\%$), while the weight has increased by only almost 2 kg ($\approx +6\%$).

Since for this case the number of design variables is too large, i.e., a number of 690 (see Tab. 3), a table with the resulting optimized design variables at point P will be dismissed. However, the structural mesh obtained and the corresponding distribution of diameters and thicknesses are shown below.

First, the original meshes created by Delaunay tesselation for both points P_5 and P_6 are depicted in Fig. 11a and Fig. 12a, respectively. Then, the optimizer defines for each individual element, values for the outer diameter and the tubular thickness. The possible values (search range) for these parameters were defined in the optimization problem. Furthermore, the optimizer tries to delete elements that are not needed, but ensures the wing profile and shape. The elements excluded for this wing at point P_5 and P_6 are shown in red in Figs 11b and 12b, respectively. Consequently, the remaining resulting structural meshes for both points are arranged in Figs. 11c and 12c.

As one may notice, the number of original mesh elements on both wings (points P_5 and P_6) were equal; however, during the optimization, the algorithm defined different thicknesses and diameters for the elements, in addition to eliminating different elements that were identified as unnecessary. Thus, Tab. 4 lists the number of elements in the original and resulting mesh for the wing models at points P_5 and P_6.

Furthermore, it is possible to illustrate the distribution of outer diameter and thickness per element for both points P_5 and P_6. Fig. 13 shows the distribution of outside diameters, where the elements in blue, red, and orange correspond to diameters of 10, 15, and 20 mm, respectively. Also, Fig. 14 shows the distribution of thicknesses, where the elements in blue, red, and orange correspond to thicknesses of 2, 4, and 6 mm, respectively.

The choice of diameter and thickness for each element follows the heuristic optimization defined by the NSGA-II. Therefore, the resultant distributions may not represent an intuitive configuration; however, at least it meets the structural and aeroelastic requirements and constraints.

Comparing the diameter and thickness distributions in Figs. 13 and 14, respectively, it is possible to notice that the

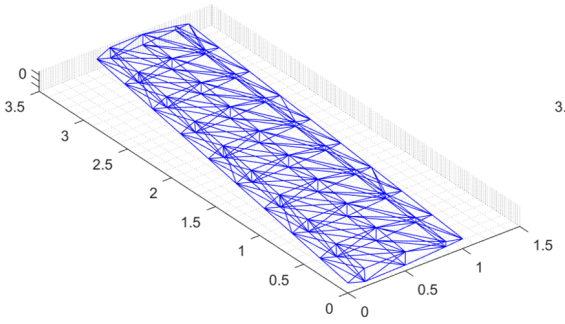

(a) Original mesh.

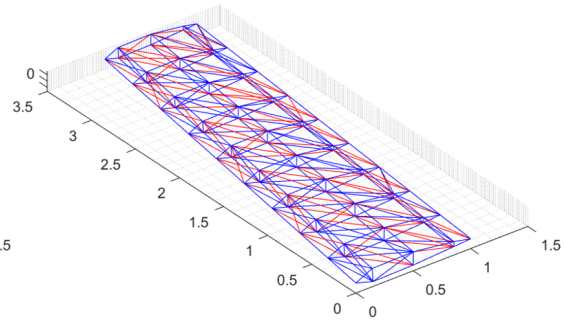

(b) Elements to be deleted in red.

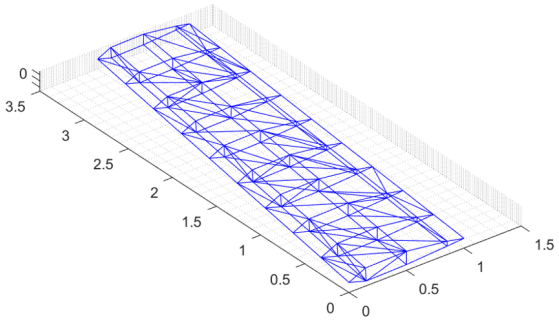

(c) Remaining mesh.

Fig. 11 Original and remaining meshes for point P_5 from Fig. 10.

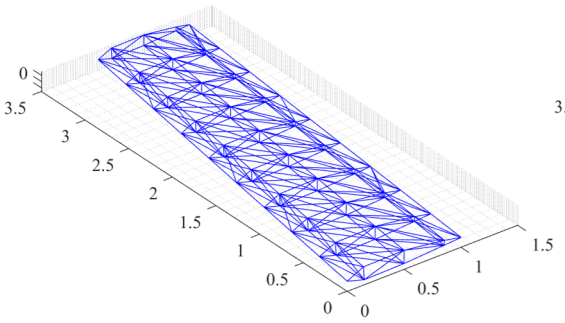

(a) Original mesh.

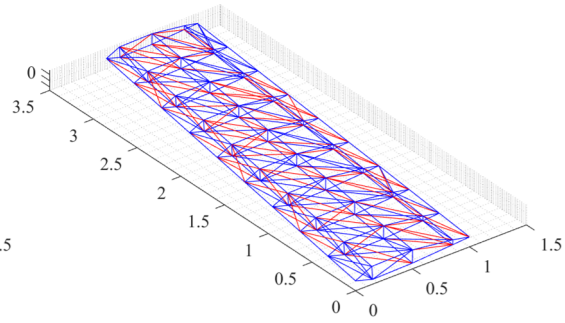

(b) Elements to be deleted in red.

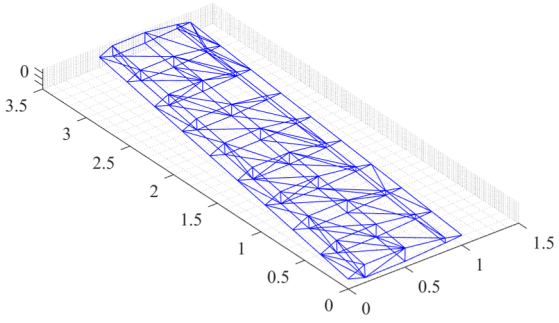

(c) Remaining mesh.

Fig. 12 Original and remaining meshes for point P_6 from Fig. 10.

Table 4 Number of elements remaining in the meshes for points P_5 and P_6.

	Point P_5	Point P_6
Number of elements in original mesh	345	345
Number of elements deleted in optimization	97	102
Number of elements in remaining mesh	243	248

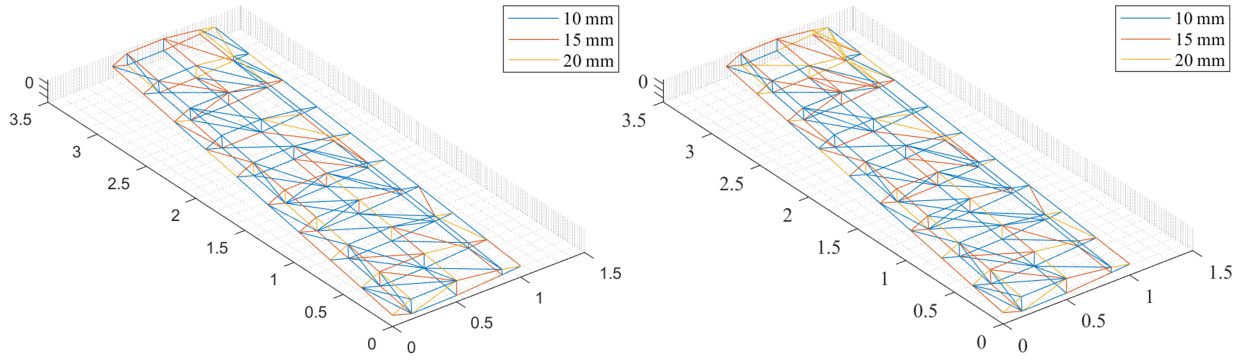

(a) Distribution for P_5. (b) Distribution for P_6.

Fig. 13 Distribution of outer diameter of each element for points P_5 and P_6 from Fig. 10.

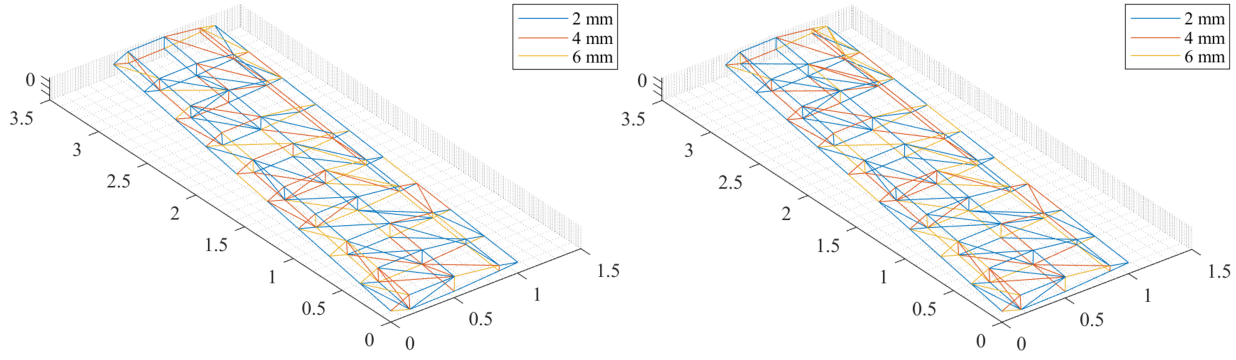

(a) Distribution for P_5. (b) Distribution for P_6.

Fig. 14 Distribution of thickness of each element for points P_5 and P_6 from Fig. 10.

wings obtained from points P_5 and P_6 change very little among themselves, so that the wing at P_6 has only 5 elements more than the wing at P_5, and the weights are very close (see Fig. 10). In addition, the distributions of diameters and thicknesses between both wings are very close, which shows that the flutter speed gain on the P_6 wing is due to specific dimension choices in some elements.

Regarding the aeroelastic solution, Fig. 15 shows the v-g-f diagrams for both points P_5 and P_6. For both points, the flutter onset happens for mode 4 due to its coupling with mode 3. Also, it can be seen that the small increase in the number of elements and the small change in the distribution of diameters and thicknesses hardly changed the initial natural frequencies; however, changes in eigenvectors generated different aeroelastic responses, which resulted in different flutter velocities.

Therefore, the optimizations presented here show different alternatives for the structural design of a wing. Modular structures, somehow, make possible new topological studies of structural meshes. However, defining the ideal topology and material properties and geometric features is still a challenge. This work, in turn, contributes to the proposed mesh generation using Delaunay and the optimization of structures. However, it is worth mentioning that the optimizations

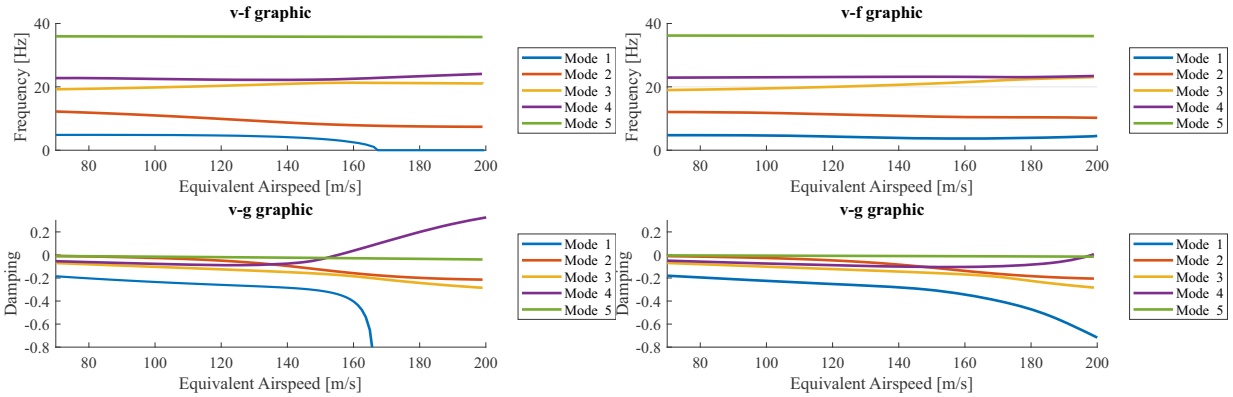

(a) V-g-f diagram for P_5.

(b) V-g-f diagram for P_6.

Fig. 15 Flutter solutions for points P_5 and P_6.

performed in this work took a long time, that is, a high computational cost; thus, better optimization time is a new challenge that will motivate future work.

Moreover, modular structures bring a range of possibilities in the structural design of wings. Among its advantages, it can be highlighted the ease of manufacture. For example, from the definition of some diameters of structures that will be used, it is possible to optimize the arrangement and the structural assembly in order to obtain the lowest weight and the best aeroelastic response. In addition, in small aircraft, such as radio-controlled aircraft or UAVs, it is possible to consider the use of modular structures manufactured in 3D printing. Such a strategy would make it possible to further increase the range of topological definitions.

IV. Concluding Remarks

This work presented a new approach to the structural design of wings, considering a new philosophy of design and definition of structures, that is, using modular structures in place of the traditional spars and ribs present in current models. In the design, structural and aeroelastic constraints were considered. Furthermore, the way these structures are spatially arranged generates a huge range of possibilities, a challenge that optimization tries to suppress.

As this work deals with the design of a wing, the Doublet-Lattice Method was used in the aerodynamic modeling and the structural modeling of the wing was performed using two types of finite elements: beam and quadrilateral elements. Furthermore, the aeroelastic problem was solved using the p-k method, helping to identify the instability and flutter conditions, which were addressed along the optimizations.

Regarding the wing design approach, a set of interpolation points is defined from an airfoil, called control points, which will be the connection nodes of the truss elements. Then, Delaunay's triangulation theory is used to generate a spatial mesh arrangement with as many elements as possible, without them intersecting. Furthermore, the choice of joint that connects these elements is essential, as it introduces mass into the system and is responsible for design constraints.

Moreover, for this study, the reference wing geometry from the FLEXOP project is used as a baseline. To improve the definition of the mesh and the dimensions of the lattice elements, two optimizations were proposed, where the objective functions were to minimize the weight of the wing and maximize the flutter speed. In the first optimization, the design variables included the number of control points in each section of the airfoil and the number of sections distributed along the wingspan. In this case, solid bar elements were considered, which resulted in very heavy designs. In the second optimization, in turn, the objective was to use tubular elements and optimize them individually, choosing for each element values of outer diameter and tubular thickness. In addition, the optimizer tried to eliminate elements that were unnecessary, in order to further reduce the weight of the structure. As the number of elements varies according to the number of nodes in each section and the section number, this work selected three pairs of parameters to generate the Paretos. It was noticed that a lower value of nodes and cross sections is able to generate a better cost-benefit in terms of weight and aeroelastic response to the structure, as long as the diameters and thicknesses are optimally combined.

Finally, this work showed how modular structures can become a great strategy in the design of aeronautical structures, specifically wings. The new wing models that are currently being presented in the literature, mainly on electric aircraft,

have increasingly thin aerodynamic profiles, since there is no longer the need to house fuel tanks. In this sense, modular structures would be interesting to lighten the structural weight of the wing and at the same time meet the structural and aeroelastic requirements. Furthermore, modular structures bring ease of fabrication as it is possible to choose some specific tube diameters and just cut the required tube sizes. Furthermore, in smaller aircraft, such as radio-controlled and UAVs, 3D printing can become an interesting alternative in the manufacture of such structures.

Acknowledgments

The authors are thankful to the Graduate Program in Mechanical Engineering of the Federal University of Uberlândia and the Brazilian Research Agencies, especially CNPq which, through process number 141753/2019-6, financially supported the work carried out.

References

[1] Wheeler, P., and Bozhko, S., "The More Electric Aircraft: Technology and challenges." *IEEE Electrification Magazine*, Vol. 2, No. 4, 2014, pp. 6–12. https://doi.org/10.1109/MELE.2014.2360720.

[2] Becken, S., and Mackey, B., "What role for offsetting aviation greenhouse gas emissions in a deep-cut carbon world?" *Journal of Air Transport Management*, Vol. 63, 2017, pp. 71–83.

[3] Naayagi, R., "A review of more electric aircraft technology," *2013 international conference on energy efficient technologies for sustainability*, IEEE, 2013, pp. 750–753.

[4] Bowman, J., Sanders, B., Cannon, B., Kudva, J., Joshi, S., and Weisshaar, T., "Development of next generation morphing aircraft structures," *48th AIAA/ASME/ASCE/AHS/ASC Structures, Structural Dynamics, and Materials Conference*, 2007, p. 1730.

[5] Velicki, A., and Jegley, D., "PRSEUS development for the hybrid wing body aircraft," *AIAA Centennial of Naval Aviation Forum" 100 Years of Achievement and Progress"*, 2011, p. 7025.

[6] Kang, M.-C., Ye, D.-H., and Go, G.-H., "International Development Trend and Technical Issues of Metal Additive Manufacturing," *Journal of Welding and Joining*, Vol. 34, No. 4, 2016, pp. 9–16.

[7] Bonet, J. T., Schellenger, H. G., Rawdon, B. K., Elmer, K. R., Wakayama, S. R., Brown, D. L., and Guo, Y., "Environmentally Responsible Aviation (ERA) Project-N+ 2 Advanced Vehicle Concepts Study and Conceptual Design of Subscale Test Vehicle (STV) Final Report," 2011.

[8] ACARE, Advisory Council for Aviation Research Innovation in Europe, "Realising Europe's vision for aviation: Strategic research innovation agenda, Vol. 1," 2012.

[9] Grönstedt, T., Xisto, C., Sethi, V., Rolt, A., García Rosa, N., Seitz, A., Yakinthos, K., Donnerhack, S., Newton, P., Tantot, N., et al., "Ultra low emission technology innovations for mid-century aircraft turbine engines," *Turbo Expo: Power for Land, Sea, and Air*, Vol. 49743, American Society of Mechanical Engineers, 2016, p. V003T06A001.

[10] Ghadge, A., Karantoni, G., Chaudhuri, A., and Srinivasan, A., "Impact of additive manufacturing on aircraft supply chain performance," *Journal of Manufacturing Technology Management*, 2018.

[11] Moore, M., "Aviation Frontiers-On Demand Aircraft," *10th AIAA Aviation Technology, Integration, and Operations (ATIO) Conference*, 2010, p. 9343.

[12] Brelje, B. J., and Martins, J. R., "Electric, hybrid, and turboelectric fixed-wing aircraft: A review of concepts, models, and design approaches," *Progress in Aerospace Sciences*, Vol. 104, 2019, pp. 1–19.

[13] Lapeña-Rey, N., Mosquera, J., Bataller, E., and Ortí, F., "First fuel-cell manned aircraft," *Journal of aircraft*, Vol. 47, No. 6, 2010, pp. 1825–1835.

[14] Nanda, A., "The propulsive design aspects on the world's first direct drive hybrid airplane," 2011.

[15] Juve, L., Fosse, J., Joubert, E., and Fouquet, N., "Airbus Group electrical aircraft program, the E-FAN project," *52nd AIAA/SAE/ASEE Joint Propulsion Conference*, 2016, p. 4613.

[16] Siemens, A., "aerobatic airplane "Extra 330LE"," *With world-record electric motor from Siemens. Press release*, 2016.

[17] Borer, N. K., Patterson, M. D., Viken, J. K., Moore, M. D., Bevirt, J., Stoll, A. M., and Gibson, A. R., "Design and performance of the NASA SCEPTOR distributed electric propulsion flight demonstrator," *16th AIAA Aviation Technology, Integration, and Operations Conference*, 2016, p. 3920.

[18] Bartels, R. E., Scott, R. C., Allen, T., and Sexton, B., "Aeroelastic analysis of SUGAR truss-braced wing wind-tunnel model using FUN3D and a nonlinear structural model," *56th AIAA/ASCE/AHS/ASC Structures, Structural Dynamics, and Materials Conference*, 2015, p. 1174.

[19] Silva, H. L., and Guimarães, T. A., "Conceptual Design of a Thin-Haul Aircraft by Energy Sizing Optimization Including Aero-Propulsive Interactions," *AIAA Scitech 2020 Forum*, 2020, p. 1503.

[20] Silva, H. L., Resende, G. J., Neto, R., Carvalho, A. R., Gil, A. A., Cruz, M. A., and Guimarães, T. A., "A multidisciplinary design optimization for conceptual design of hybrid-electric aircraft," *Structural and Multidisciplinary Optimization*, 2021, pp. 1–22.

[21] Tariq, M., Maswood, A. I., Gajanayake, C. J., and Gupta, A. K., "Aircraft batteries: current trend towards more electric aircraft," *IET Electrical Systems in Transportation*, Vol. 7, No. 2, 2016, pp. 93–103.

[22] "Airbus reveals new zero-emission concept aircraft," *Airbus*, 2020. URL https://www.airbus.com/newsroom/press-releases/en/2020/09/airbus-reveals-new-zeroemission-concept-aircraft.html.

[23] Trainelli, L., Comincini, D., Salucci, F., Rolando, A., and Riboldi, C., "Sizing and performance of hydrogen-driven airplanes," *Proc. XXV AIDAA Congress, Roma, Italy*, 2019.

[24] Drela, M., "Development of the D8 transport configuration," *29th AIAA Applied Aerodynamics Conference*, 2011, p. 3970.

[25] Bradley, M. K., and Droney, C. K., "Subsonic ultra green aircraft research," 2011.

[26] Martins, J., Kennedy, G., and Kenway, G. K., "High aspect ratio wing design: Optimal aerostructural tradeoffs for the next generation of materials," *52nd Aerospace Sciences Meeting*, 2014, p. 0596.

[27] Zhang, J.-k., Li, Z.-n., and Kou, C.-h., "Structural Design of High Aspect Ratio Composite Material Wing (P)," *ACTA AERONAUTICA ET ASTRONAUTICA SINICA-SERIES A AND B-*, Vol. 26, No. 4, 2005, p. 450.

[28] Afonso, F., Vale, J., Oliveira, É., Lau, F., and Suleman, A., "A review on non-linear aeroelasticity of high aspect-ratio wings," *Progress in Aerospace Sciences*, Vol. 89, 2017, pp. 40–57.

[29] Österheld, C., Heinze, W., and Horst, P., "Influence of aeroelastic effects on preliminary aircraft design," *Proceedings of the ICAS-Congress, Harrogate*, 2000.

[30] Saleem, W., Yuqing, F., and Yunqiao, W., "Application of Topology Optimization and Manufacturing Simulations-A new trend in design of Aircraft components," *Proceedings of the International MultiConference of Engineers and Computer Scientists*, Vol. 2, Citeseer, 2008.

[31] Sleesongsom, S., Bureerat, S., and Tai, K., "Aircraft morphing wing design by using partial topology optimization," *Structural and Multidisciplinary Optimization*, Vol. 48, No. 6, 2013, pp. 1109–1128.

[32] Montemurro, M., Vincenti, A., and Vannucci, P., "A two-level procedure for the global optimum design of composite modular structures—application to the design of an aircraft wing," *Journal of Optimization Theory and Applications*, Vol. 155, No. 1, 2012, pp. 24–53.

[33] Moses, E., Fuchs, M., and Ryvkin, M., "Topological design of modular structures under arbitrary loading," *Structural and Multidisciplinary Optimization*, Vol. 24, No. 6, 2002, pp. 407–417.

[34] Sodja, J., Werter, N., and De Breuker, R., "Design of a flying demonstrator wing for manoeuvre load alleviation with cruise shape constraint," *2018 AIAA/ASCE/AHS/ASC Structures, Structural Dynamics, and Materials Conference*, American Institute of Aeronautics and Astronautics, Reston, Virginia, 2018. https://doi.org/10.2514/6.2018-2153, URL https://arc.aiaa.org/doi/10.2514/6.2018-2153.

[35] Brockman, R. A., "Dynamics of the bilinear Mindlin plate element," *International Journal for Numerical Methods in Engineering*, Vol. 24, No. 12, 1987, pp. 2343–2356. https://doi.org/10.1002/nme.1620241208, URL http://doi.wiley.com/10.1002/nme.1620241208.

[36] Adam, F. M., Mohamed, A. E., and Hassaballa, A. E., "Degenerated Four Nodes Shell Element with Drilling Degree of Freedom," *IOSR Journal of Engineering*, Vol. 3, No. 8, 2013, pp. 10–20. URL http://www.iosrjen.org.

[37] Luo, Y., "An Efficient 3D Timoshenko Beam Element with Consistent Shape Functions," *Adv. Theor. Appl. Mech.*, Vol. 1, No. 3, 2008, pp. 95–106.

[38] Castro, S. G. P., "General-purpose finite element solver based on Python and Cython," , 2022. DOI: https://doi.org/10.5281/zenodo.6573490.

[39] Albano, E., and Rodden, W. P., "A doublet-lattice method for calculating lift distributions on oscillating surfaces in subsonic flows." *AIAA journal*, Vol. 7, No. 2, 1969, pp. 279–285.

[40] Geising, J., Kalman, T., and Rodden, W., "Subsonic Unsteady Aerodynamics for General Configurations, Part 1, Vol. 1-Direct Application of the Nonplanar Doublet-Lattice Method," *AFFDL TR-71-5*, , No. Part 1, ????

[41] Blair, M., "A compilation of the mathematics leading to the doublet lattice method," Tech. rep., WRIGHT LAB WRIGHT-PATTERSON AFB OH, 1992.

[42] Wright, J. R., and Cooper, J. E., *Introduction to aircraft aeroelasticity and loads*, Vol. 20, John Wiley & Sons, 2008.

[43] Hassig, H. J., "An approximate true damping solution of the flutter equation by determinant iteration." *Journal of Aircraft*, Vol. 8, No. 11, 1971, pp. 885–889.

[44] Opgenoord, M. M., and Willcox, K. E., "Design methodology for aeroelastic tailoring of additively manufactured lattice structures using low-order methods," *AIAA Journal*, Vol. 57, No. 11, 2019, pp. 4903–4914. DOI: https://doi.org/10.2514/1.J058169.

[45] Süelözgen, Ö., and Wüstenhagen, M., "OPERATIONAL MODAL ANALYSIS FOR SIMULATED FLIGHT FLUTTER TEST OF AN UNCONVENTIONAL AIRCRAFT¨Ozge," *International Forum on Aeroelasticity and Structural Dynamics*, 2019.